Mon. Not. R. Astron. Soc. **380,** 657–664 (2007) doi:10.1111/j.1365-2966.2007.12096.x

Figure rotation of dark haloes in cold dark matter simulations

S. E. Bryan[1] and C. M. Cress[1,2]★

[1]*Astrophysics and Cosmology Research Unit, University of KwaZulu-Natal, Westville, South Africa*
[2]*Physics Department, University of the Western Cape, Private Bag X17, 7535 Bellville, South Africa*

Accepted 2007 June 7. Received 2007 May 29; in original form 2006 August 31

ABSTRACT

We investigate the figure rotation of dark matter haloes identified in Λ cold dark matter (CDM) simulations. We find that when strict criteria are used to select suitable haloes for study, five of the 222 haloes identified in our $z = 0$ simulation output undergo coherent figure rotation over a 5 h^{-1} Gyr period. We discuss the effects of varying the selection criteria and find that pattern speeds for a much larger fraction of the haloes can be measured when the criteria are relaxed. Pattern speeds measured over a 1 h^{-1} Gyr period follow a lognormal distribution, centred at $\Omega_{\rm p} = 0.2\,h$ rad Gyr^{-1} with a maximum value of 0.94 h rad Gyr^{-1}. Over a 5 h^{-1} Gyr period, the average pattern speed of a halo is about 0.1 h rad Gyr^{-1} and the largest pattern speed found is 0.24 h rad Gyr^{-1}. Less than half of the selected haloes showed alignment between their figure rotation axis and minor axis, the exact fraction being somewhat dependent on how one defines a halo. While the pattern speeds observed are lower than those generally thought capable of causing spiral structure, we note that coherent figure rotation is found over very long periods and argue that further simulations would be required before strong conclusions about spiral structure in all galaxies could be drawn. We find no correlation between halo properties such as total mass and the pattern speed.

Key words: methods: *N*-body simulations – galaxies: haloes – galaxies: kinematics and dynamics – dark matter.

1 INTRODUCTION

Initially, calculations of stellar orbits in galaxies ignored the dark matter halo completely. Then, as observational evidence for dark matter haloes increased (Gunn 1980), orbit calculations involved modelling the haloes as stationary spherical objects. Further investigation into dark matter haloes indicated that many haloes were in fact triaxial (Dubinski & Carlberg 1991; Warren et al. 1992) and not spherical. This was taken into consideration in, for example, Schwarzschild (1993) but orbits were still modelled within stationary dark matter haloes and these calculations fail to take into account the effect of figure rotation. Bekki & Freeman (2002) suggest that figure rotation of the dark halo would play an important role in the formation and evolution of the embedded galaxies. In particular, they suggest that figure rotation may influence the formation of stellar bars as well as spiral arms and warps. They also suggest that figure rotation could trigger star bursts in galaxies, even at high redshifts. Since orbits passing near the centre of galaxies are affected, figure rotation could also have consequences for black hole growth in galaxies (de Zeeuw & Franx 1991) and the so-called 'cusp/core problem' (de Blok et al. 2001). Observations of such effects could be used to constrain current galaxy formation theories.

★Email: cressc@ukzn.ac.za

Initial work on the subject of figure rotation was done by Dubinski in 1992. He found that haloes in simulations which included tidal effects experienced a notable rotation. The haloes were found to have pattern speeds ranging from 0.1 to 1.6 radians per Gyr. (These units are essentially equivalent to km s^{-1} kpc^{-1}.) The small sample size and somewhat artificial implementation of the tidal field meant further studies in this area were necessary. Pfitzner (1999) noted that a significant number of triaxial haloes produced in cold dark matter (CDM) simulations tended to rotate steadily around their minor axes. One such halo was extracted from the simulation at late times and was allowed to evolve in isolation over a 5 Gyr period. During this time, the halo was found to rotate as a solid body with constant speed of about 1.1 radians per Gyr. In 1999, Bureau et al. (1999) proposed that slow figure rotation of a surrounding triaxial dark halo may be responsible for creating the spiral structure seen in NGC 2915 and encouraged further studies of gas discs contained within the potentials of rotating triaxial dark haloes. Bekki & Freeman (2002) continued this work, using numerical simulations. They showed that a 'slowly' rotating triaxial dark halo could cause large spiral arms in an extended gas disc, and that the resulting structure is strongly dependent on the pattern speed of the halo. Masset & Bureau (2003) further explored the effects of a rotating triaxial dark halo proposed by Bureau et al. (1999) using hydrodynamical simulations and concluded that, while a rotating triaxial halo could be responsible for causing spiral structure, the

required pattern speed was prohibitively large – between 5.5 and 6.5 radians per Gyr.

More recently, Bailin & Steinmetz (2004, hereafter BS04) compared the orientation of the major axis determined from the central sphere (radius of 0.6 × virial radius) of 317 haloes selected from a high-resolution simulation over five time intervals (a total period of just over 1 Gyr). They found that 278 (88 per cent) of their haloes did indeed rotate smoothly, with pattern speeds of around 0.15 h (where $H_0 = 100\,h$ km s^{-1} Mpc^{-1}) radians per Gyr. They noted that the pattern speeds observed in the inner regions of the undisturbed haloes in their sample were not sufficient to cause the spiral patterns as discussed by Bureau et al. (1999).

We note that the simulations of Masset & Bureau (2003) are 2D and the code used was usually applied to discs around stars. When one considers the 3D simulations of Bekki & Freeman (2002), in their fig. 2(f), some spiral structure is evident after 1 Gyr for much smaller pattern speeds than those considered by Masset & Bureau (2003). The slowest figure rotation in Bekki & Freeman (2002) is 0.77 km s^{-1} kpc^{-1}, which is significantly larger than typical values found in BS04, but it is unclear what would be expected in galaxies with slower pattern speeds over much longer periods of time. Here, we extend the analysis of BS04 to investigate whether one would expect coherent figure rotation over periods much longer than the 1 Gyr period they used.

We have simulated the evolution of structure in a $(50\,h^{-1}$ Mpc$)^3$ region of space, in a ΛCDM cosmology, using the N-body code GADGET (Springel, Yoshida & White 2001) to evolve the positions and velocities of 256^3 collisionless particles. Haloes are identified from the simulation using a friends-of-friends algorithm (FoF). To explore figure rotation, we have identified haloes from simulation outputs at a redshift of zero and then traced them back through time. We then determine the principal axes of each halo using the inertia tensor. By following the motion of the principal axes of each halo over several time steps, we are able to measure the pattern speed of the halo. Our approach is similar to that of BS04 but we extend their analysis to test some of their assumptions.

This paper is laid out as follows. In Section 2, the simulations and analysis procedure are described. In Section 3, we present the results of the analysis: the mass function, the spin parameter distribution, the outcome of halo tracing and the accretion constraints applied, the outcome of substructure elimination, the environment of haloes selected for study, the figure rotation measurements, the alignment between rotation axis and the minor axis and, finally, the correlation between the pattern speed and halo properties, such as halo mass. In Section 4 we discuss the results.

2 METHODOLOGY

2.1 Initial conditions

We assume the standard model for structure formation: that density fluctuations are Gaussian and the initial power spectrum is given by a power law, $P_0 \propto k^n$, where $n \sim 1$. As the universe moves from a radiation-dominated to a matter-dominated phase and fluctuations begin to grow, the power spectrum becomes modified in a way that depends on the density of dark matter. Bardeen et al. (1986) give the transfer function T [where $P(k) = P_0(k)$ T] for a universe that is dominated by CDM. The normalization of the spectrum can be obtained from observations of the Cosmic Microwave Background or from the measured abundance of clusters of galaxies. To set initial particle positions and velocities, we used the COSMICS package (van de Weygaert & Bertschinger 1996) with $\Omega_{\rm m} = 0.3$, $\Omega_\Lambda = 0.7$ and $\sigma_8 = 0.9$.

Table 1. Simulation parameters.

Parameter	Parameter value
$N_{\rm particles}$	256^3
Box length	$50\,h^{-1}$ Mpc
$M_{\rm particle}$	$6.2 \times 10^8\,h^{-1}\,{\rm M}_\odot$
Force softening	$30\,h^{-1}$ kpc
Initial redshift	55

2.2 Simulations

We ran the publicly available parallel version of GADGET on a cluster of eight 2 GB machines. Doing so allowed us to follow the evolution of 256^3 particles. We have chosen to simulate a cube of length $50\ h^{-1}$ Mpc. This is sufficiently large to produce reliable periodic simulations (Power et al. 2003). The choice of particle number and volume means that in this simulation each dark matter particle has a mass of $\sim 6 \times 10^8\,{\rm M}_\odot$. Guided by studies of Athanassoula et al. (2000), we have used a force softening of $30\ h^{-1}$ kpc to prevent numerical instability. The parameters chosen for our simulation are summarized in Table 1.

2.3 Analysis procedure

We have identified haloes (groups of 10 or more particles) in the redshift zero snapshot using FoF, a simple FoF group finder for N-body simulations developed by the simulation group at the University of Washington. We have used the common convention of setting our linking length to be 0.2 times the mean inter-particle spacing. We obtained results for two different definitions of a halo. First, we used all particles identified by the group finder and relied on our technique for substructure elimination to exclude groups which contained 'subhaloes'. We also tried the halo definition of BS04, which selects a central sphere of particles within a group. Once we have defined which particles are in a halo, we use the positions of these particles to calculate the inertia tensor, and hence the principal axes, of the halo of interest at each time-step.

2.3.1 Calculating the inertia tensor

For figure rotation analysis, we model each halo as a rigid body, and calculate the inertia tensor using

$$I_{ij} = \sum_\alpha m_\alpha \left[\delta_{ij} \sum_k x_{\alpha,k}^2 - x_{\alpha,i} x_{\alpha,j} \right].$$

The eigenvalues and eigenvectors of this tensor are then extracted using Jacobi transformations. We have also performed the figure rotation analysis using the modified inertia tensor suggested by BS04, which artificially weights central particles in haloes.

2.3.2 Tracing haloes through time and accretion constraints

To follow halo properties with redshift, we need to associate each halo with its progenitor haloes at a previous time-step. This is done with merger trees using code developed by Kauffmann et al. (1999). The algorithm begins at the first output time, z_i, at which a halo (of

10 or more particles) can be found. It then steps through all haloes identified at the next output time, z_{i+1}, searching for progenitor haloes in the z_i output. A halo at redshift z_i is said to be a progenitor of a halo at redshift z_{i+1} if, and only if, two conditions are satisfied.

(i) A progenitor halo at z_i must contribute at least half of its particles to the halo at z_{i+1} and

(ii) the central (most gravitationally bound) particle of the progenitor halo at z_i must be contained within the halo at z_{i+1} .

We then step through haloes in the z_{i+2} output, searching for progenitors in the z_{i+1} time-step. This continues until the output time of $z = 0$ is reached.

Once a merger tree has been established, we exclude haloes which have accreted a significant fraction of their mass over the time period considered. In the 'halo matching' technique of BS04, they excluded haloes which accreted more than 15 per cent of their mass over a $1\,h^{-1}$ Gyr period; that is, to be considered for figure rotation analysis, a halo at $z = 0$ must contain at least 85 per cent of the particles contained by the largest progenitor halo identified in the time-step which is $1\,h^{-1}$ Gyr earlier.

Since we extend our analysis to consider haloes over a much longer period of time, we have explored the effects of relaxing this limit over the 3 and $5\,h^{-1}$ Gyr period and include haloes which accrete as much as 25 per cent of their mass over $3\,h^{-1}$ Gyr and 30 per cent over $5\,h^{-1}$ Gyr. We then consider the consequences of relaxing the constraint even further in our 5 h^{-1} Gyr analysis: instead of comparing particles in a halo at $z = 0$ with the largest progenitor halo identified 5 h^{-1} Gyr before, we impose a constraint on progenitor haloes at each successive time-step. Thus, at each time-step, haloes must contain at least 70 per cent of the particles contained by the largest progenitor halo in the previous time-step.

2.3.3 Measuring the figure rotation of a halo

To determine the figure rotation of the halo, we then followed a plane fitting approach suggested by BS04, where a detailed description of the method is given. Briefly, the method involves fitting a plane to the principal axes of the halo of interest determined over several time-steps and then solving for the plane, $z = ax + by$, that best fits these axes. Once the plane has been determined, measuring the amount of rotation in the plane is straightforward. The principal axis is projected on to the plane at each time-step and the angle between the projected principal axes over a time interval gives the figure rotation of the halo. We then used linear regression to find the best-fitting linear relation for this figure rotation, the slope giving the pattern speed of the halo.

We have also measured the figure rotation of several haloes using the method described by Dubinski (1992) and found that these results are similar to the ones we obtain using the plane fitting approach.

3 RESULTS

Many of the results from this section are summarized in Table 2.

3.1 Mass function

The mass function is a measure of the number of haloes as a function of their mass. Jenkins et al. (2001) were able to predict the mass distribution of dark haloes expected in a CDM universe by combining the results from several *N*-body simulations. The fit obtained by Jenkins et al. (2001) shows good agreement with the theoretical predictions of the Sheth and Tormen formula (Sheth & Tormen 1999). The mass function obtained from our simulation is shown in Fig. 1. This figure is a log plot of the number of haloes as a function of their mass in the $(50\,h^{-1}\,\mathrm{Mpc})^3$ region of our simulation, at a redshift of zero. We have found that our mass function agrees well with that of Jenkins et al. (2001) over the range of haloes simulated.

3.2 Angular momentum

We use the computationally convenient expression for the spin parameter, defined by Bullock et al. (2001) as

$$\lambda' \equiv \frac{J}{\sqrt{2}\,M\,V\,R} \tag{1}$$

to calculate the spin parameter of each of our simulated haloes. This expression describes the spin parameter for a sphere of radius R (taken to be the virial radius), where M is the mass contained within the sphere, J is the angular momentum of the sphere and V is the circular velocity at the radius R. Fig. 2 shows the distribution of the spin parameter found in our simulation. The spin parameter was calculated for all simulated haloes which have more than 200 particles ($M > 10^{11}\,h^{-1}\,\mathrm{M}_{\odot}$). The curve is the lognormal distribution given by

$$P(\lambda') = \frac{1}{\lambda'\sqrt{2\,\pi}\sigma}\,\exp\left[-\frac{\ln^2\left(\frac{\lambda'}{\lambda'_0}\right)}{2\,\sigma^2}\right] \tag{2}$$

with best-fitting values of $\lambda'_0 = 0.034 \pm 0.003$ and $\sigma = 0.62 \pm 0.08$. We have found that our best-fitting value for λ'_0 and σ is consistent with the values obtained by Barnes & Efstathiou (1987) and Bullock et al. (2001).

Table 2. Summary of results. Values given in the first four rows correspond to the number of haloes, of the original 222, which remain after various cuts are made. The accretion cut is applied before the substructure cut. We give results for two different methods of doing the substructure cut. Values given in the last three rows are for the first substructure cut, not that of BS04. The fitted value of μ is also given in units of radians per gigayear. Only the mean is given for the $5\,h^{-1}$ Gyr sample since it only includes five haloes.

	$1\,h^{-1}$ Gyr	$3\,h^{-1}$ Gyr	$5\,h^{-1}$ Gyr	$5\,h^{-1}$ Gyr relaxed
Haloes traced	218	201	191	191
Haloes after accretion cut	183	62	13	74
Haloes after substructure cut	115	38	5	48
Haloes after BS04 substructure cut	89	55	12	70
Coherent figure rotation	61 per cent	71 per cent	100 per cent	73 per cent
μ (fitted)	-0.60 ± 0.03	-0.95 ± 0.04	-1.03	-0.94 ± 0.02
μ (rad Gyr^{-1})	0.25 h	0.11 h	0.09 h	0.11 h
σ	0.37 ± 0.03	0.27 ± 0.04		0.21 ± 0.02

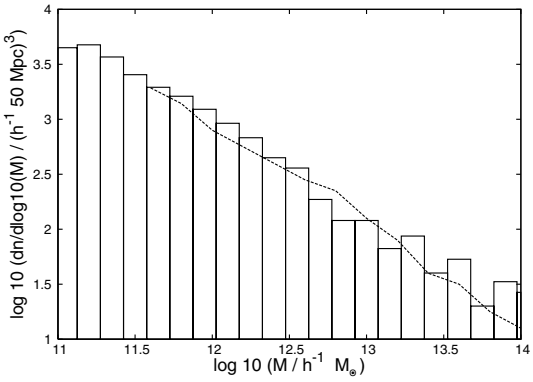

Figure 1. The mass function. The histogram shows the number of haloes as a function of the halo mass in the simulated region at redshift zero and the line shows the fit obtained by Jenkins et al. (2001).

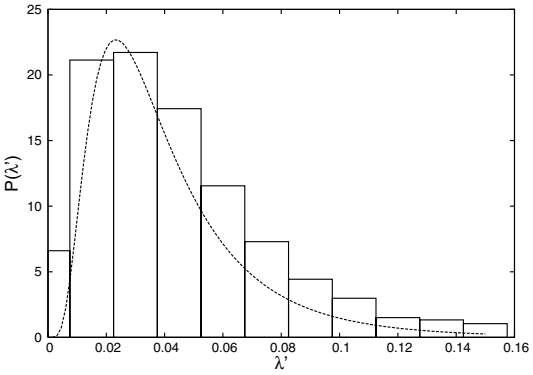

Figure 2. This figure shows the distribution of the dimensionless spin parameter λ' for all simulated haloes containing at least 200 particles, together with the lognormal distribution given by equation (2) with fitted parameters $\lambda'_0 = 0.034 \pm 0.003$ and $\sigma = 0.62 \pm 0.08$.

3.3 Halo tracing and accretion constraint results

BS04 used a computationally intensive bootstrapping technique to show that the error in the determination of a halo's principal axes depends on the number of particles contained within that halo and the intrinsic shape of the halo. They also showed that it was not possible to measure the principal axes of haloes with the precision required for figure rotation measurements if the haloes contained fewer than 4000 particles. Guided by their work, we identified the 222 haloes in our simulation at a redshift of zero, which contain at least 4000 particles (i.e. a mass of at least $2.5 \times 10^{12}\, h^{-1}\, \mathrm{M}_{\odot}$). BS04 also showed that errors are large for haloes which are almost oblate but this only affects a small number of haloes in our case. We are able to trace 218, 201 and 191 haloes over the 1, 3 and $5\, h^{-1}$ Gyr periods, respectively.

After imposing constraints on the acceptable amount of accretion over the time period considered, as discussed in Section 2.3.2, we are left with samples of 183, 62 and 13 haloes over the 1, 3 and $5\, h^{-1}$ Gyr periods, respectively. When we use the relaxed $5\, h^{-1}$ Gyr constraints, i.e. impose a constraint at each time-step, rather than a constraint over the entire period, we obtain 74 haloes over $5\, h^{-1}$ Gyr.

3.4 Eliminating haloes with substructure

We are concerned with the figure rotation of undisturbed haloes and, therefore, need to eliminate all haloes exhibiting a significant amount of substructure. Identifying substructure is somewhat subjective and we compared various methods. The first method involved projecting the distribution of particles along three perpendicular axes and considering each axis individually. We expect the mass distribution of an undisturbed halo to be smooth when considered along any axis and the presence of a secondary peak in this distribution thus provides evidence of substructure. We calculated the mass contained in bins moving out from the centre of the halo, where the centre is defined as the most bound particle. If any bin contained more mass than an inner bin, we compared the mass of that bin to the total mass of the halo. After visually inspecting the distributions, and some experimentation, we chose to use 25 bins and eliminate haloes if an outer bin contained more than 10 per cent of the total halo mass. Applying this to our sample of haloes over a period of $1\, h^{-1}$ Gyr, we eliminated 68 haloes on the basis of substructure. 24 and eight haloes needed to be excluded from the sample over the 3 and $5\, h^{-1}$ Gyr periods, respectively. For our larger $5\, h^{-1}$ Gyr sample, where we constrain common particles between successive time-steps, 26 of the 74 haloes need to be eliminated.

We also tried using the method of BS04. Their method involves excluding haloes if the calculated pattern speed varies significantly when one changes the size of the sphere used to define a halo. The BS04 method only considers particles within the central sphere of the halo and substructure outside of this will not cause a halo to be eliminated. Using this approach, we found that 94, seven and one of the 183, 62 and 13 haloes we considered would have been eliminated. For the relaxed constraint over $5\, h^{-1}$ Gyr, four of the 74 haloes need to be eliminated. We note that our method was generally more conservative over longer time periods (over the $5\, h^{-1}$ Gyr period we rejected 35 per cent of haloes while 5 per cent would have been eliminated using their method) but there were a few haloes that would have been excluded using their method and were not excluded using ours.

3.5 Mass density in surrounding environment

In order to explore the environment of our haloes, we have considered the mass density of the area surrounding the haloes at $z = 0$. To do this we have, for each halo, found the number of particles within $5\, h^{-1}$ Mpc of the halo. The sum of the surrounding mass is then divided by the volume of a sphere with radius of $5\, h^{-1}$ Mpc. The results are shown in Fig. 3 where we plot the fraction of haloes as a function of the log of their mass density. The top figure shows the distribution of mass density of all the haloes identified from the simulation, while the bottom histogram shows the distribution of our sample of undisturbed haloes. While we lose a few of the most massive haloes in our selection, the undisturbed haloes appear to occur in an environment which is slightly more dense than average. This is consistent with the results of Gottlöber, Klypin & Kravtsov (2001) who found that, for $z < 1$, the merger rate of cluster haloes to be three times lower than that of isolated haloes and twice as low as haloes that end up in groups. With this in mind, we expect that undisturbed haloes would occur in a more dense environment.

3.6 Figure rotation

To determine the pattern speed of a halo, we have followed each halo over a period of $5\, h^{-1}$ Gyr (or 1 or $3\, h^{-1}$ Gyr if the halo does

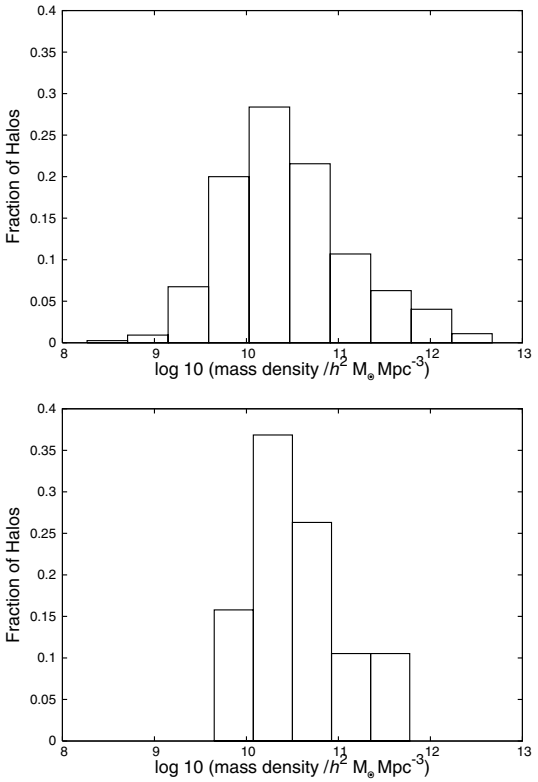

Figure 3. The mass density in surrounding environment. These histograms show the fraction of haloes versus the log of the mass density of the surrounding environment. Top: the surrounding environment of all simulated haloes. Bottom: the environment of the haloes selected for 3 Gyr analysis.

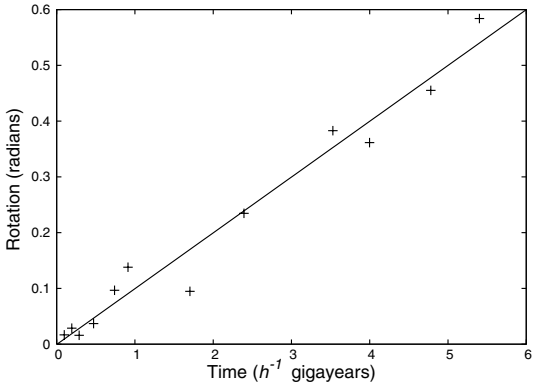

Figure 4. Pattern speed of a single halo measured over $5\,h^{-1}$ Gyr. Each point represents the angle (in radians) that the figure has rotated over the time interval given. The slope of this plot (obtained by linear regression) gives the pattern speed of the halo.

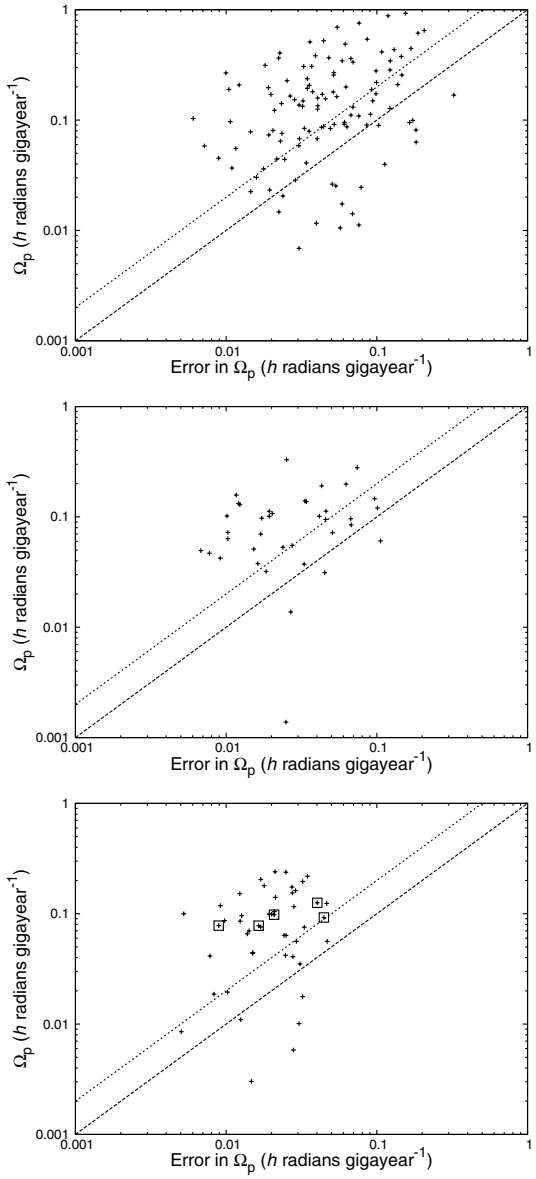

Figure 5. Measured pattern speeds of the simulated haloes versus the estimated error in pattern speed. The dashed line represents the points at which the pattern speed is equal to the estimated error (1σ limit) and the dotted line represents the points at which the pattern speed is equal to twice the error. Haloes with pattern speeds less than twice the error are not considered to be rotating coherently. Top: haloes considered over $1\,h^{-1}$ Gyr period. Centre: haloes considered over $3\,h^{-1}$ Gyr. Bottom: haloes considered over $5\,h^{-1}$ Gyr period using relaxed accretion constraints. Boxed crosses mark the pattern speeds and errors of the five haloes that meet the stricter accretion criteria similar to that used in the top and middle plots and in BS04.

not satisfy selection criteria over longer periods). Using linear regression, we have found the best-fitting linear relation for the figure rotation of the haloes as a function of time. The pattern speed of the halo is given by the slope of the linear fit. We have calculated the 1σ limit of the slope, and we have taken this to be the error in the pattern speed. Fig. 4 shows the figure rotation of one of our haloes that has remained unaffected by substructure over a $5\,h^{-1}$ Gyr period. Results are similar for other haloes. A linear fit is adequate over the whole period and there is no indication that the pattern speeds are systematically changing over time.

Fig. 5 shows the pattern speeds obtained for our haloes. The 115 haloes observed over $1\,h^{-1}$ Gyr are shown in the top plot, the middle plot shows the 38 haloes observed over $3\,h^{-1}$ Gyr and the bottom plot shows the haloes considered to be undisturbed over $5\,h^{-1}$ Gyr period using relaxed accretion constraints (boxed crosses mark the pattern speeds and errors of the five haloes that meet the stricter accretion criteria similar to that used in the top and middle plots and in BS04). The x-axis is the estimated error in pattern speeds. The dashed line represents the points at which the observed pattern speed is equal to the estimated error. We have also shown the points

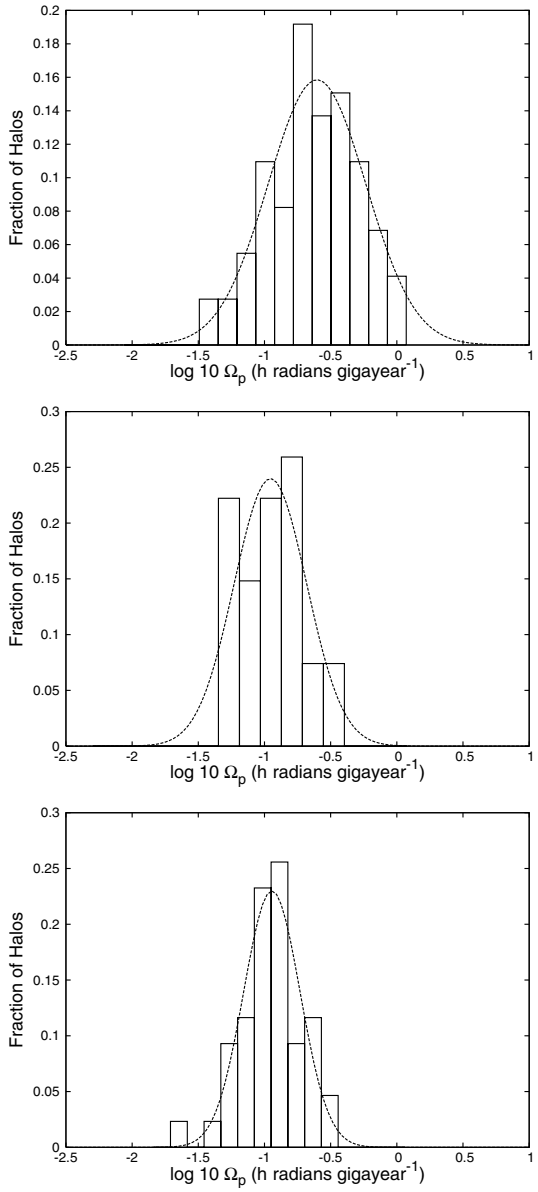

Figure 6. Pattern speed distribution for rotating haloes. This histogram shows the distribution of the pattern speeds calculated from our undisturbed haloes. The line is the lognormal distribution (equation 3). Top: haloes rotating over 1 h^{-1} Gyr (best-fitting values of $\mu = -0.60 \pm 0.03$ and $\sigma = 0.37 \pm 0.03$). Centre: haloes rotating over 3 h^{-1} Gyr ($\mu = -0.95 \pm 0.04$ and $\sigma = 0.27 \pm 0.04$). Bottom: haloes rotating over 5 h^{-1} Gyr (relaxed constraints) ($\mu = -0.94 \pm 0.02$ and $\sigma = 0.21 \pm 0.02$).

at which the pattern speed is equal to twice the estimated error (dotted line). Using a 2σ cut-off for haloes to be considered rotating coherently, 63 per cent of the haloes in the 1 h^{-1} Gyr sample, 71 per cent of the haloes in the 3 h^{-1} Gyr and 100 (73) per cent of the haloes in the 5 h^{-1} Gyr(relaxed) sample exhibit coherent figure rotation.

We found that the distribution of pattern speeds of the undisturbed haloes from our simulation was fairly well fit by the lognormal distribution

$$P(\Omega_{\rm p}) = \frac{1}{\Omega_{\rm p}\,\sigma\,\sqrt{2\,\pi}}\,\exp\left[\frac{-\log^2\left(\frac{\Omega_{\rm p}}{\mu}\right)}{2\,\sigma^2}\right]. \quad (3)$$

Fig. 6 shows the distribution of pattern speeds for the haloes considered, together with the lognormal distribution (equation 3). Best-fitting values to this curve are given in Table 2. For the undisturbed haloes over 5 h^{-1} Gyr, the fastest figure rotation detected was 0.13 h radians per Gyr and the average pattern speed of these haloes was 0.09 h radians per Gyr. The maximum figure rotation for the haloes with relaxed constraints over 5 h^{-1} is 0.24 h radians per Gyr. Adjusting our cut-off to include only those haloes with pattern speeds greater than three times the error does not significantly change the pattern speed distribution.

3.7 Alignment between figure rotation axis and minor axis

Dubinski (1992), Pfitzner (1999) and BS04 all noted that for the majority of their simulated haloes the major axis appeared to rotate around the minor axis. To explore this, we have determined the dot product between the figure rotation axis and the minor axis of each of the haloes in our sample. Fig. 7 shows our results when we use a standard inertia tensor and do not limit ourselves to central particles in the definition of the halo. It appears that these axes are well aligned for at least a third of the haloes. We note, however, that the fraction of haloes exhibiting this alignment is smaller than in other studies. If we consider only the spherical centre of the haloes, the percentage of haloes exhibiting this alignment increases to ∼50 per cent which is more consistent with the 58 per cent found by BS04. Using a modified inertia tensor also slightly increases the fraction of haloes found to be rotating around the minor axis.

3.8 Effect of halo properties on pattern speed

We have investigated the correlation of pattern speed with halo properties such as mass, density of the surrounding environment and the amount of matter accreted over 5 h^{-1} Gyr (fraction of particles common to progenitor and current haloes). We plot results in Fig. 8, demonstrating that pattern speed is not correlated with any of these halo properties. The final plot demonstrates that our results are not sensitive to the accretion cut values we use.

4 DISCUSSION AND CONCLUSIONS

We have found that the mass function determined from our simulation is well fit by the mass function obtained by Jenkins et al. (2001) using *N*-body simulations. The distribution of the spin parameter found from our simulation was well fit by a lognormal distribution (equation 2) with a best-fitting value of $\lambda_0' = 0.034$. This agrees well with the values found by Barnes & Efstathiou (1987) and Bullock et al. (2001). Both of these tests suggest that the simulations we have run are reliable, agreeing with many previous simulations as well as with theoretical predictions.

We selected haloes which had not accreted a large fraction of their material and which did not show evidence for significant substructure and found that 63 per cent of the 115 haloes considered over 1 h^{-1} Gyr did exhibit coherent figure rotation, where 'coherent' is arbitrarily defined to be pattern speeds greater than two times the estimated error. The distribution of the pattern speeds over 1 h^{-1} Gyr was well fit by a lognormal distribution centred at $\log(\Omega_{\rm p}) = -0.60 \pm 0.01$ ($\Omega_{\rm p} = 0.24h$ radians per Gyr). The pattern speeds of these haloes, determined over a 1 h^{-1} Gyr period, are consistent with the lower end of the 0.1–1.6 radians per Gyr found by Dubinski (1992), but slower than the 1.1 radians per Gyr detected by Pfitzner (1999). Our distribution of pattern speeds peaks at slightly higher values than those found by BS04, but the difference is not very significant. It appears that limiting oneself to the central sphere of a

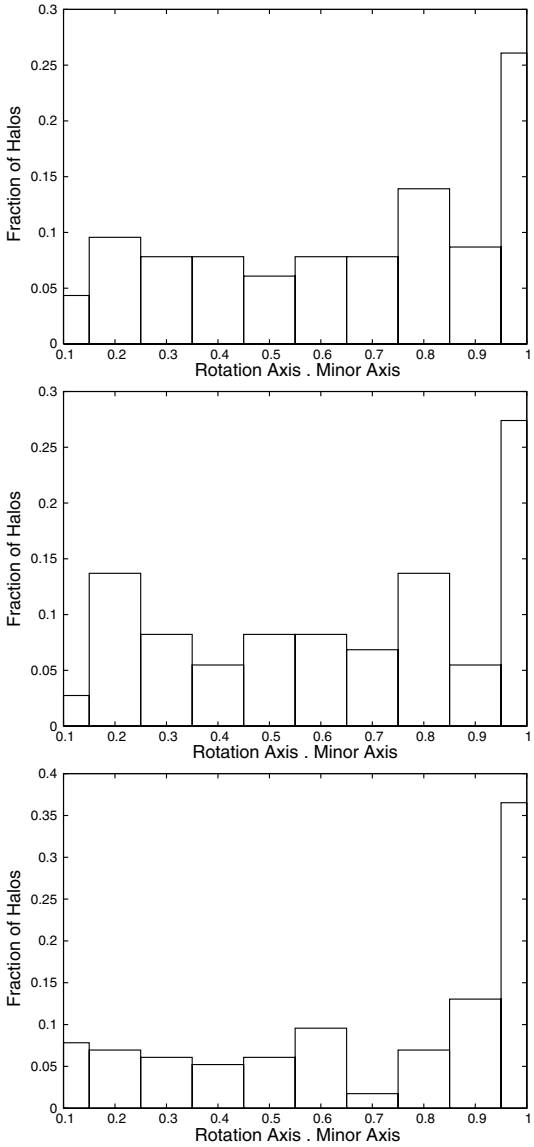

Figure 7. Alignment between figure rotation axis and minor axis. This figure shows the dot product of the figure rotation axis and the minor axis. Top: axes calculated for the 115 haloes in our sample using the whole halo and the 'standard' inertia tensor. Middle: axes calculated for the 73 haloes found to undergo coherent rotation. Bottom: axes (for 115 haloes) calculated using a central sphere of 0.6 times the virial radius and a modified inertia tensor.

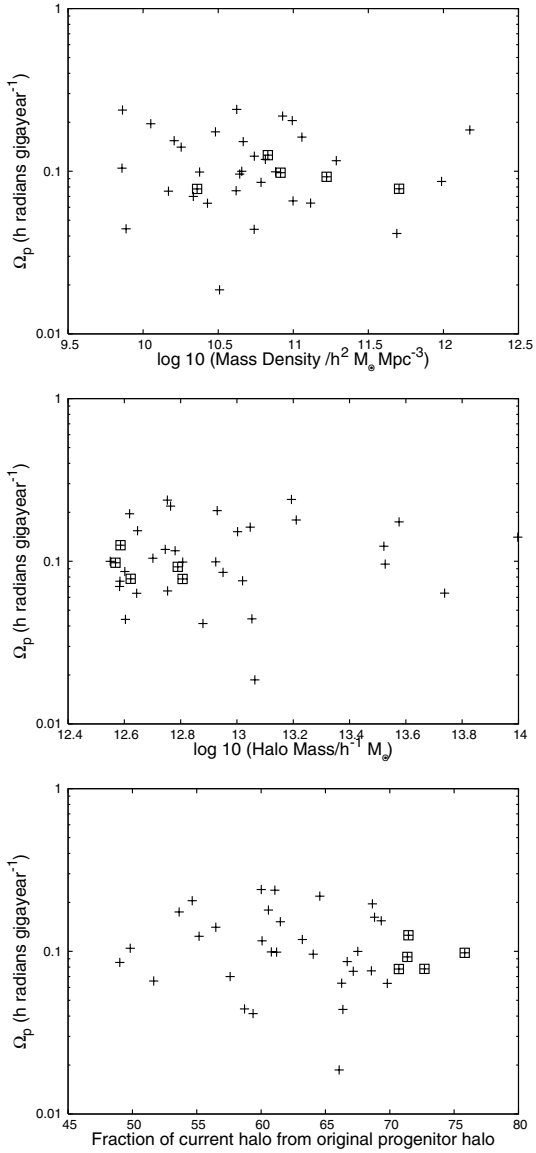

Figure 8. Pattern speed versus halo properties. We have compared pattern speeds to (from top to bottom) the mass density in the surrounding environment, the halo mass and the fraction of current halo particles present in progenitor halo. The pattern speeds are calculated over the $5\,h^{-1}$ Gyr period. The halo mass and mass density in surrounding environment are determined at $z = 0$. Boxed crosses are haloes which meet the stricter accretion criteria of BS04.

group and using a modified inertia tensor do not significantly influence the results. The accretion cut and the substructure cut affect the number of haloes considered, but the pattern speed distributions are not very sensitive to the details.

The pattern speed distributions appear to shift to lower speeds as one looks over longer periods. The difference between the 3 and $5\,h^{-1}$ Gyr distributions is not significant but the difference between the 1 and $5\,h^{-1}$ Gyr distributions is significant. This result holds no matter what halo definition, accretion cut or method of substructure removal is used. Presumably, studying the haloes over a longer time period allows us to detect smaller figure rotations above the noise but, over $5\,h^{-1}$ Gyr, there are no haloes with the larger figure rotations seen over $1\,h^{-1}$ Gyr, suggesting that accretion and/or mergers allow for increased pattern speeds. In general, the speeds found are much slower than those Masset & Bureau (2003) claim are required for spiral structure in NGC 2915 but, given the long periods of time over which these haloes show coherent figure rotation and the results of Bekki & Freeman (2002), we suggest that further hydro-simulations would be required before strong conclusions can be drawn for all galaxies.

The sample of undisturbed haloes we have chosen for analysis is generally found to be in more dense environments than the average haloes in the simulation. This is consistent with the results of Gottlöber et al. (2001) who suggest that, at low redshifts ($z < 1$), the merger rate is lower in denser environments.

In studying the relationship between the figure rotation axis and the minor axis, we found alignment for many of the haloes but a significant fraction which were not very well aligned. The two axes

are within 25° of each other in 30 per cent of the haloes, using the 'whole-group' definition of a halo. If we restricted our analysis to the central region and used the modified inertia tensor, as did BS04, our results are more similar to theirs.

We have found no correlation between halo properties such as halo mass, or environment, and the pattern speed.

ACKNOWLEDGMENTS

The financial assistance of the South African National Research Foundation (NRF) towards this research is hereby acknowledged. Opinions expressed and conclusions arrived at are those of the author and are not necessarily to be attributed to the NRF.

REFERENCES

Athanassoula E., Fady E., Lambert J. C., Bosma A, 2000, MNRAS, 314, 475
Bailin J., Steinmetz M., 2004, ApJ, 616, 27 (BS04)
Bardeen J., Bond J., Kaiser N., Szalay A., 1986, ApJ, 304, 15
Barnes J., Efstathiou G., 1987, ApJ, 319, 575
Bekki K., Freeman K., 2002, ApJ, 574, L21
Bullock J. S., Dekel A., Kolatt T. S., Kravtsov A. V., Klypin A. A., Porciani C., Primack J. R., 2001, ApJ, 555, 240
Bureau M., Freeman K., Pfitzner D., Meurer G., 1999, AJ, 118, 2158
de Blok W. J. G., McGaugh S. S., Bosma A., Rubin V. C., 2001, ApJ, 69, 103
de Zeeuw T., Franx M., 1991, ARA&A, 29, 239
Dubinski J., 1992, ApJ, 401, 441
Dubinski J., Carlberg R. G., 1992, ApJ, 378, 496
Gottlöber S., Klypin A., Kravtsov A. V., 2001, ApJ, 546, 223
Gunn J. E., 1980, R. Soc. Lond. Phil. Trans. Ser. A, 296, 313
Jenkins A., Frenk C. S., White S. D. M., Colberg J. M., Cole S., Evrard A. E., Couchman H. M. P., Yoshida N., 2001, MNRAS, 321, 372
Kauffmann G., Colberg J. M., Diaferio D., White S. D. M., 1999, MNRAS, 303, 188
Masset F., Bureau M., 2003, ApJ, 586, 152
Pfitzner D., 1999, PhD thesis, Australian National Univ.
Power C., Navarro J. F., Jenkins A., Frenk C. S., White S. D. M., Springel V., Stadel J., Quinn T., 2003, MNRAS, 338, 14
Schwarzschild M., 1993, ApJ, 409, 563
Sheth R. K., Tormen G., 1999, MNRAS, 308, 119
Springel V., Yoshida N., White S. D. M., 2001, New Astron., 6, 79
Warren M. S., Quinn P. J., Salmon J. K., Zurek W. H., 1992, ApJ, 399, 405
van de Weygaert R., Bertschinger E., 1996, MNRAS, 281, 84

This paper has been typeset from a TEX/LATEX file prepared by the author.